The 2016 World Congress on
Advances in Civil, Environmental, and Materials Research (ACEM16)
Jeju Island, Korea, August 28-September 1, 2016

Size Distribution and Magnetic Optimization of Phase Pure Chromium Doped Magnetite Nanoparticles

*Zaheer H Shah[1)], Saira Riaz[2)], Zohra N Kayani[3)] and *Shahzad Naseem[4)]

[1), 2), 4)] Centre of Excellence in Solid State Physics, University of the Punjab, QAC, Lahore-54590, Pakistan
[1)] Department of Physics, UMT, Lahore, Pakistan
[3)] Department of Physics, LCWU, Lahore, Pakistan
[4)] shahzad.cssp@pu.edu.pk

ABSTRACT

Functional iron oxide nanostructures have been of particular interest during the last decade for their remarkable properties which makes them suitable for broad range of applications. Un-doped and chromium doped iron oxide nanoparticles (NPs) have been synthesized using sol-gel method. Dopant concentration is varied as 1-9%. XRD results confirm the formation of hematite phase in un-doped and Cr-doped NPs. Shift in peak position, to higher angles, might have been observed because of the lower ionic radius of Cr (61.4pm) as compared to iron (74pm). Dielectric constant remains constant at low frequencies and increases as frequency of applied field is increased to 10MHz. Such type of variation in dielectric constant is associated with space charge polarization. Increase in dielectric constant till dopant concentration of 7% arises due to reduction in grain size to 35nm. It can be seen through cole-cole plots that because of high resistance of grain boundaries, resistance of grain and grain boundaries cannot be separated. VSM results show increase in saturation magnetization as dopant concentration is increased to 7%.

1. INTRODUCTION

Demand of iron oxides nanostructures at industrial level is increased day by day due to attractive applications in cancer diagnosis and therapy, fabrication of biocompatible magnetic fluids, electrochemical devices, lithium ion batteries and many more (Sivula et al. 2010, Arico et al. 2005, Ali et al. 2015). Recently, iron oxide nano electrodes are extensively using in lithium ion batteries (LIBs) with high specific energy density and long life cycle (Bruce et al. 2008). Among all the iron oxides, alpha iron oxide (α-Fe_2O_3) attracted the material researchers because of its immense properties, huge abundance in nature, high theoretical specific capacity and cost effectiveness (Chen et al. 2014, Wang et al. 2013). α-Fe_2O_3 with n-type semiconducting properties have wide range of applications in the field of environment treatment, solar cells, electrochemical devices, drug delivery vehicles and water remediation (Yavuz et al. 2006, Wang et al. 2001, Zhang et al. 2010). Owing to such large applications, there is

one problem with α-Fe_2O_3 that is its weak magnetic effects. Therefore, to enhance the magnetic coercivity and magnetic saturation, various metals have been doped in α-Fe_2O_3.

One dimension α-Fe_2O_3 nanostructures have been synthesized of different shapes, i.e. nano-rods, nanotubes, nanowires and nano-belts using various types of experimental techniques. Besides, some porous and mesoporous iron oxide nanoparticles were also fabricated for different applications (Jia et al. 2005, Yan et al. 2011). Mostly, porous materials are widely used to sense toxic and explosive gases. Furthermore, α-Fe_2O_3 nano materials have also enhanced dielectric properties with theoretically investigated band gap E_g = 2.2 eV (Riaz et al. 2014a, Akbar et al. 2014a).

Up to now, there are different experimental techniques that have been adopted to get α-Fe_2O_3 nano materials. In the present work, pure and Cr-doped α-Fe_2O_3 nanoparticles have been prepared using wet chemical sol-gel method. Moreover, effects on the grain size and grain boundaries by substitution of Cr doping has been investigated. It was observed in this study that incorporation of Cr in α-Fe_2O_3 enhanced the magnetic and dielectric properties.

2. EXPERIMENTAL DETAILS

Pure and doped α-Fe_2O_3 nanoparticles were synthesized via sol gel method. The stoichiometric amount of starting materials was weighed using made and model electronic balance. The homogeneous mixture of precursors was made in deionized water (DI). The solution was put on hot plate and transferred into the ESCO fume hood. The solution was heated in definite intervals of temperature which led to sol formation. The sol was heated to obtain nanoparticles.

Further, different characterization techniques were used to study the various properties of as-synthesized nanoparticles. The crystal size and structure of samples was investigated by Bruker D8 Advance X-ray diffractometer (XRD) with CuK_α (1.5406Å) radiations. Lake Shore's 7407 vibrating sample magnetometer (VSM) examined the magnetic properties. Dielectric properties were analyzed with the help of 6500 Precision impedance analyzer.

3. RESULTS AND DISCUSSION

XRD spectrum of as-prepared Cr-doped (3%, 5%, 7% and 9%) α-Fe_2O_3 samples is shown in Fig. 1. The data retrieved from X-ray diffractometer was manipulated and indexed. It exhibits phase pure Cr-doped α-Fe_2O_3. The XRD pattern revealed that as doping level increased from 3 % to 9% diffraction peaks shifted to larger angles and became more intense. The most elevated diffraction peaks, (104), (110), (024) and (116) proved the formation of hexagonal crystal structure. The shift in peak position, to higher angles, might have been observed due to small ionic radius of Cr (61.4pm) as compared to Fe (74pm). This leads to reduction in lattice parameters and unit cell volume as observed in Table 1.

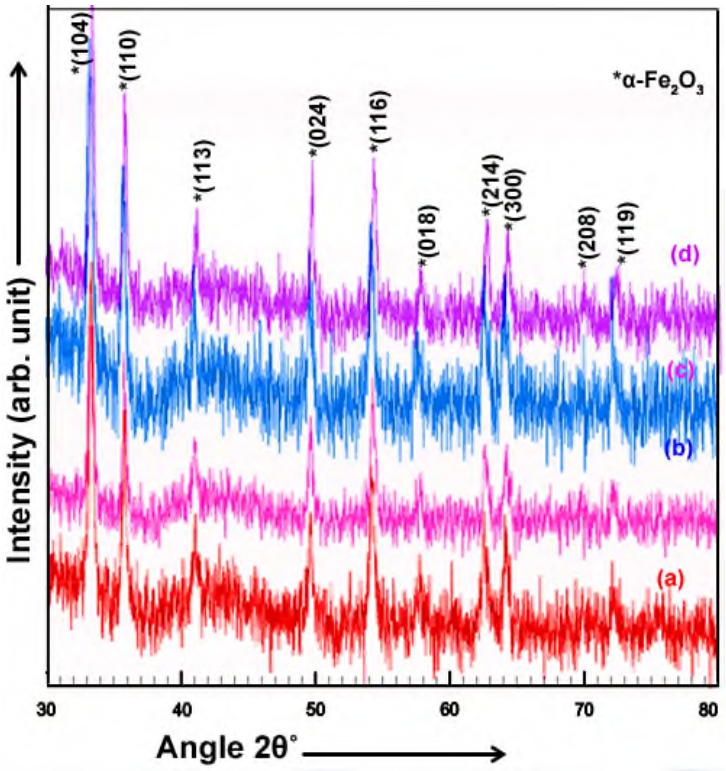

Fig. 1 XRD patterns for Cr doped Fe_2O_3 nanoparticles with dopant concentration (a) 3% (b) 5% (c) 7% (d) 9%

Table 1 Lattice parameters and unit cell volume for Cr doped Fe_2O_3 nanoparticles

Dopant concentration (%)	Lattice parameters (Å)		Unit cell volume (Å^3)
	a	c	
3	5.025	13.650	298.4851
5	5.023	13.643	298.0946
7	5.022	13.638	297.8667
9	5.019	13.625	297.2274

Crystallite size (t) (Cullity 1956) and dislocation density (δ) (Kumar et al. 2011) were calculated using Eqs. 1-2

$$t = \frac{0.9\lambda}{B\cos\theta} \quad (1)$$

$$\delta = \frac{1}{t^2} \quad (2)$$

Where, θ is the diffraction angle, λ is the wavelength (1.5406Å) and B is Full Width at Half Maximum, d_{exp} is the d-spacing calculated using XRD patterns. Dislocation density decreases with increase in dopant concentration to 7% accompanied by increase in crystallite size. This decrease in dislocation density

indicates that dopant atoms are dissolved in α-Fe_2O_3 lattice. At high dopant concentration increased dislocation density and decreased crystallite size is attributed to the dopant atoms that takes place on the grain boundaries.

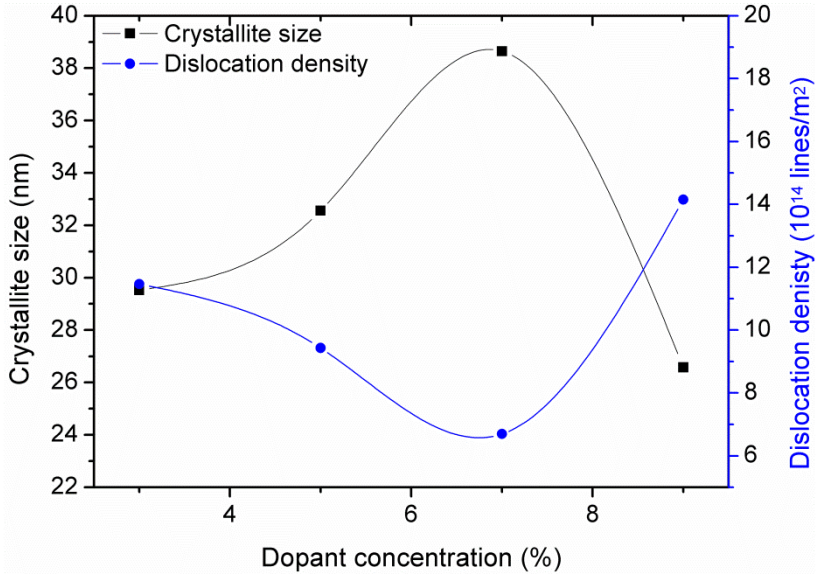

Fig.2 Crystallite size and dislocation density plotted as a function of dopant concentration

Frequency dependent dielectric constant of iron oxide nanoparticles has been obtained by using impedance analyzer manufactured by Wayne Kerr. All measurements were taken at room temperature in the frequency range of 1k – 20 MHz. It is observed from the graph in Fig. 3 that in the lower frequency range the dielectric constant seems to be frequency independent while as the frequency increases from 10 MHz an exponential increase in the dielectric constant is observed. Such increase in dielectric constant in the high frequency range makes these materials promising candidate to be used in high frequency devices in microwave range. This increment can be justified on the basis of Koop's theory, according to which all dielectric materials are made up of two layers one of them is of conducting grains and the second one is of non-conducting grain boundaries (Barsoukov and Macdonald 2005). According to this theory, at low frequency conducting grains are more active than non-conducting grain boundaries. But as the frequency approaches to 1MHz the behavior of grains and grain boundaries flips and grain boundaries dominates over grains and thus dielectric constant increases (Barsoukov and Macdonald 2005). Further adding, when frequency of the applied field becomes equal to the jumping frequency of ions dielectric constant can be increased (Barsoukov and Macdonald 2005) as observed in our case. It can be seen in inset Fig. 3 that dielectric constant increases from 62.5 (log f = 5.5) to 66.2 (log f = 5.5) as dopant concentration was increased from 3% to 7%. This increase in dielectric constant is associated with increase in crystallite size and decrease in dislocation density.

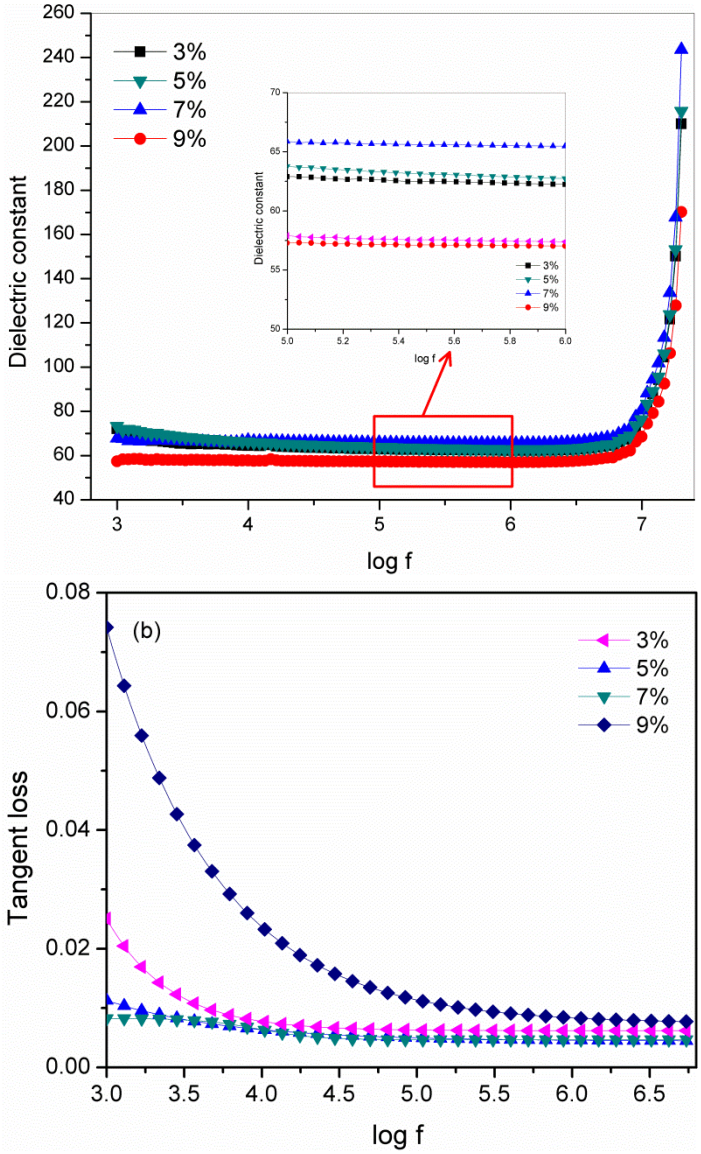

Fig. 3 Dielectric constant and tangent loss for Cr doped iron oxide nanoparticles

The impedance spectroscopy is a powerful technique for investigating the electrical properties such as conductivity, dielectric behavior and relaxation characteristics of the electro-ceramic nanoparticles. This impedance analysis permits researchers to find the contributions of different processes such as bulk effects and grain boundaries. Fig. 4 shows the complex impedance plane plot of 7% and 9% dopant concentrations. Impedance plots of polycrystalline materials are generally characterized by the appearance of one or more semicircles. These semicircles depend upon different relaxation effects present in the system (Barsoukov and Macdonald 2005). The diameter of each circle on Z' axis shows the resistance of individual's relaxation phenomenon. According to Koop's theory grain boundaries are more resistive than grains because of the present of high density of structural and chemical

defects. Thus semicircle appearing at low frequency shows the resistance of grains and the other one appearing at high frequency give the resistance of grain boundaries (Barsoukov and Macdonald 2005). But in our case because of high resistance of grain boundaries we cannot distinguish the resistance of grains and grain boundaries due to high resistance of grain boundaries (Barsoukov and Macdonald 2005).

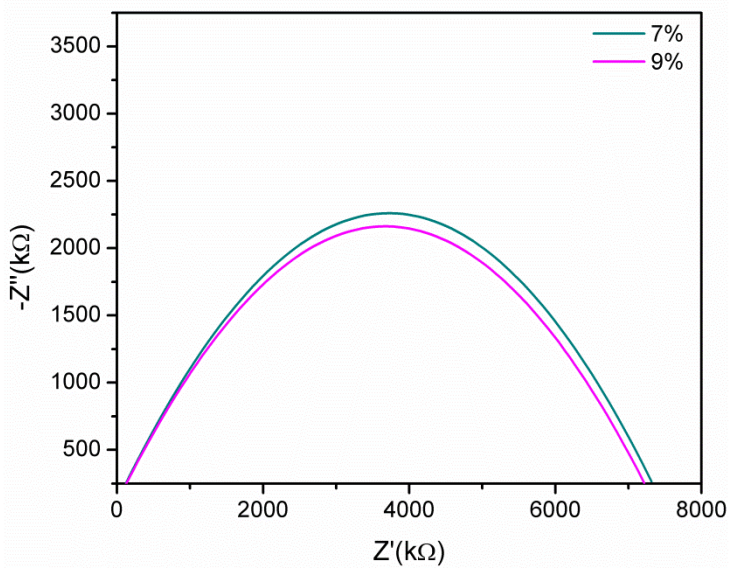

Fig. 4 Cole-Cole plot of chromium doped iron oxide nanoparticles

Fig. 5 shows M-H curves for Cr doped α-Fe_2O_3 nanoparticles. Cr doped α-Fe_2O_3 nanoparticles exhibit ferromagnetic behavior. Replacement of Cr in place of Fe sites results in the presence of magnetic moments that are localized around a site. This increases the inequality between the two sublattices of α-Fe_2O_3 thus increasing the magnetization. At dopant concentration 9%, likelihood of having Cr ions that are free in the host lattice increases. This results in decreased magnetization (Riaz et al. 2014a, Akbar et al. 2014a). In addition, with the presence of two sublattices, like in hematite structure, spins experience ferromagnetic coupling within the same plane while antiferromagnetic coupling arises with the spins of adjacent planes. Extra d electron obtained as dopant replace the host atom will take the direction of localized spins. This results in an extra electron with spin up that cannot hop to the neighboring site (Riaz et al. 2014). But this type of hopping is favorable in our case supported by increase in magnetization with doping upto 7%.

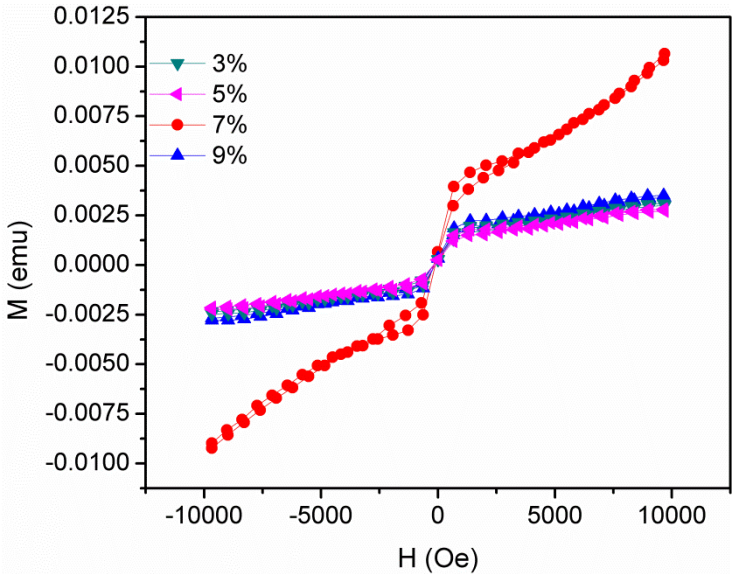

Fig. 5 M-H curves for Cr doped iron oxide nanoparticles

4. CONCLUSIONS

Cr doped α-Fe_2O_3 nanoparticles were prepared with dopant concentration 3%, 5%, 7% and 9% using sol-gel method. XRD results showed successful incorporation of dopant in the α-Fe_2O_3 lattice. Dielectric constant increased at high frequencies while tangent loss decreased at high frequencies. Cr doped α-Fe_2O_3 nanoparticles showed ferromagnetic behavior. Highest dielectric constant and highest saturation magnetization were achieved at dopant concentration 7%.

REFERENCES

Akbar, A., Riaz, S., Ashraf, R. and Naseem, S. (2014(b)), "Magnetic and magnetization properties of Co-doped Fe_2O_3 thin films," *IEEE Trans. Magn.*, **50**, 2201204

Akbar, A., Riaz, S., Bashir, M. and Naseem, S. (2014a), "Effect of Fe^{3+}/Fe^{2+} Ratio on Superparamagnetic Behavior of Spin Coated Iron Oxide Thin Films," *IEE Trans. Magn.*, **50**, 2200804.

Ali, K. Sarfraz, A. K. Mirza, I. M. Bahadur, A. Iqbal, S. Haq, A. (2015), "Preparation of superparamagneticmaghemite (g-Fe_2O_3) nanoparticles by wet chemical route and investigation of their magnetic and dielectric properties." *Cur. App. Phy.* **15**, 925-929.

Arico, S. Bruce, P. Scrosati, B. Tarascon, J. M. and Van, S. W. (2005), "Nanostructured materials for advanced energy conversion and storage devices." *Nat. Mater.* Vol**4**, 366-377.

Barsoukov, E. and Macdonald, J.R. (2005), "Impedance Spectroscopy Theory, Experiment, and Applications," John Wiley & Sons, Inc., Publication, New Jersey, 2005.

Bruce, P. G. Scrosati, B. and Tarascon, J. M. (2008), “Nanomaterials for rechargeable lithium batteries.” *Angew. Chem. Int. Ed.* **47**, 2930-2946.

Chen, L. Xu, H. Li, L. Wu, F. Yang, J. and Qian, Y. (2-14), “A comparative study of lithium storage, performances of hematite: nanotubes vs. nanorods.” *J. Power. Sources.* Vol.**245,** 429-435.

Cullity, B.D. (1956), “Elements of x-ray diffraction,” Addison Wesley Publishing Company, USA.

Jia, C. J. Sun, L. D. Yan, Z. G. You, L. P. Luo, F. Han, X. D. Pang, Y. C. Zhang, Z. and Yan, C. H. (2005), “Single-crystalline iron oxide nanotubes.” *Angew. Chem. Int. Ed.* **44**, 4328–4333.

Kumar, N., Sharma, V., Parihar, U., Sachdeva, R., Padha, N. and Panchal, C.J. (2011) “Structure, optical and electrical characterization of tin selenide thin films deposited at room temperature using thermal evaporation method,” *J. Nano- Electron. Phys.*, **3**, 117-126

Riaz, S., Akbar, A. and Naseem, S. (2014a), “Ferromagnetic Effects in Cr-Doped Fe_2O_3 Thin Films,” *IEEE Trans. Magn.*, **50**, 2200704

Riaz, S., Ashraf, R., Akbar, A. and Naseem, S. (2014b), “Free Growth of Iron Oxide Nanostructures by Sol-Gel Spin Coating Technique—Structural and Magnetic Properties,” *IEE Trans. Magn.*, **50**, 2301805

Sivula, K. Zboril, R. Formal, F. L. Robert, R. Weidenkaff, A. Tucek, J. Frydrych, J. and Gratzel, M. (2010), “Photoelectrochemical water splitting with mesoporous hematite prepared by a solution-based colloidal approach.” *J. Am. Chem. Soc.* **132**, 7436-7444.

Wang, C. Wang, L. and Tang, K. (2013), “Synthesis of mesoporous Fe_2O_3nanorods and their electrochemical performance.” *Int. J. Electrochem. Sci.* **8**, 4543-4550.

Wang, Z. Hu, X. Käll, P. O. Helmersson, U. (2001), "High Li^+-Ion storage capacity and double-electro chromic behavior of sol-gel derived iron oxide thin films with sulfate residues.” *Chem. Mater.* **13**, 1976-1983.

Yan, L. Fan, H. Zhai, Y. Yang, C. Ren, P. and Huang, L.(2011), ‘Low temperature solution-based synthesis of porous flower-like -Fe_2O_3 superstructures and their excellent gas-sensing properties.” *Sens. Actuators B: Chem.* **160**(1), 1372–1379.

Yavuz, C. T. Mayo, J. T. Yu, W. W. Prakash, A. Falkner, J. C. Yean, S. Cong, L. Shipley, H. J. Kan, A. Tomson, M. Natelson, D. andColvin, V. L. (2006), “Low-field magnetic separation of monodisperse Fe_3O_4 nanocrystals.” **314**(5801), 964-967.

Zhang, G. Gao, Y. Zhang, Y. and Guo, Y. (2010), “Fe_2O_3-pillared recto rite as an efficient and stable fenton-like heterogeneous catalyst for photo degradation of organic contaminants.” *Environ. Sci. Technol.* **44**,6384-6389.